A Frequency and Polarization Reconfigurable Circularly Polarized Antenna Using Active EBG Structure for Satellite Navigation

Bin Liang, Benito Sanz-Izquierdo, Edward A. Parker, and John C. Batchelor, *Senior Member, IEEE*

***Abstract*—This paper presents a broadband frequency tunable and polarization reconfigurable circularly polarized (CP) antenna, using a novel active electromagnetic band gap (EBG) structure. The EBG surface employs identical metallic rectangular patch arrays on both sides of a thin substrate, but rotated by 90° from each other. The active bias circuits are also orthogonal for each surface, enabling the reflection phases for orthogonal incident waves to be tuned independently in a wide frequency range. By placing a wideband coplanar waveguide (CPW) fed monopole antenna above the EBG surface, and properly tuning the bias voltages across the varactors in each direction, CP waves can be generated at any desired frequency over a broad band. In accordance with simulations, the measured 3 dB axial ratio (AR) bandwidth reaches 40% (1.03–1.54 GHz), with good input matching (S_{11}) and radiation patterns at six presented sampling frequencies. The polarization reconfigurability is verified by simulations and measurements, and shown to be capable of switching between left hand circular polarization (LHCP) and right hand circular polarization (RHCP).**

***Index Terms*—Broadband antenna, circular polarization (CP), electromagnetic band gap (EBG), reconfigurable, varactor.**

I. Introduction

ELECTROMAGNETIC BAND GAP (EBG) structures have drawn great interests in field of electromagnetics for many years [1]–[3]. Owing to the distinctive properties of surface wave suppression in a frequency band gap and zero-phase reflection coefficient for certain incident waves, EBGs have been broadly used in various antenna applications [4]–[7]. In [8], the feature of reflection coefficient phase dependency on incident wave polarization was exploited to develop the polarization-dependent EBG (PDEBG). In [9], this attractive characteristic was employed to generate circularly polarized (CP) radiation pattern. By using a PDEBG structure as the ground plane with rectangular patch unit cells on top, the linearly polarized (LP) wave radiated by a simple dipole was converted to CP.

In recent years, since CP antennas are desired in many applications of wireless communication and satellite navigation, studies of [9] were further developed. Reference [10] proposed a dual-band PDEBG surface as a reflector for a dual-band dipole antenna to realize dual-band CP, with left hand CP (LHCP) at 3.4 GHz and right hand CP (RHCP) at 6.4 GHz respectively. In [11], a microstrip antenna above an EBG structure using rectangular unit cells was presented. By truncating the corners of the microstrip antenna and the use of a PDEBG, broadband characteristics around 6 GHz were achieved. Although these developments have extended the performance of [9] into dual-band or broadband, the flexibility of these antennas is still limited.

Varactor diodes in EBG structures have been widely used to achieve dynamic flexibility [12]–[19]. As the capacitance of varactors is changed with the bias voltage, the working frequency of the EBG can be electrically tuned. In [12], a varactor was loaded on the radiating edge of each microstrip patch element, connecting the patch and the ground plane, while in [13] and [14], varactors were placed between adjacent square patches. The bias voltages of cells could be varied individually in both of these two designs, although multiple layers are required because of the vias. To simplify the structure and the biasing connection, a design based on the configuration in [3] was presented in [15], adopting a resistive-lumped-element biasing grid that was introduced in [16]. In this design, vias were also required in order to provide uniform bias voltages. Alternatively, [17]–[19] presented another biasing technique with no vias between the element and ground, where adjacent square patches were connected with a thin metal track to provide DC continuity. The connecting lines were perpendicular to the direction of the varactors, so that the structure was active only in the polarization parallel to the direction of the diodes.

In this paper, a new dual-polarized tunable EBG is proposed, in which the reflection phase of orthogonally polarized incident plane waves can be tuned independently. The EBG surface incorporates a very thin flexible substrate with periodic rectangular patches etched into metal cladding on its two sides, and also including surface varactors and resistors. The double-sided structure has been used in much recent research [20]–[23], offering a high level of reconfiguration. Vias are not required in the design for the bias circuit or to suppress surface waves. In

Manuscript received June 25, 2014; revised September 04, 2014; accepted October 20, 2014. Date of publication November 05, 2014; date of current version December 31, 2014. This work was supported by the China Scholarship Council (CSC).

B. Liang is with the Microwave Engineering Laboratory, Beihang University, Beijing 100191, China and also with the School of Engineering and Digital Arts, University of Kent, Canterbury CT2 7NT, U.K. (e-mail: bl213@kent.ac.uk).

B. Sanz-Izquierdo, E. A. Parker, and J. C. Batchelor are with the School of Engineering and Digital Arts, University of Kent, Canterbury CT2 7NT, U.K. (e-mail: b.sanz@kent.ac.uk).

Color versions of one or more of the figures in this paper are available online at http://ieeexplore.ieee.org.

Digital Object Identifier 10.1109/TAP.2014.2367537

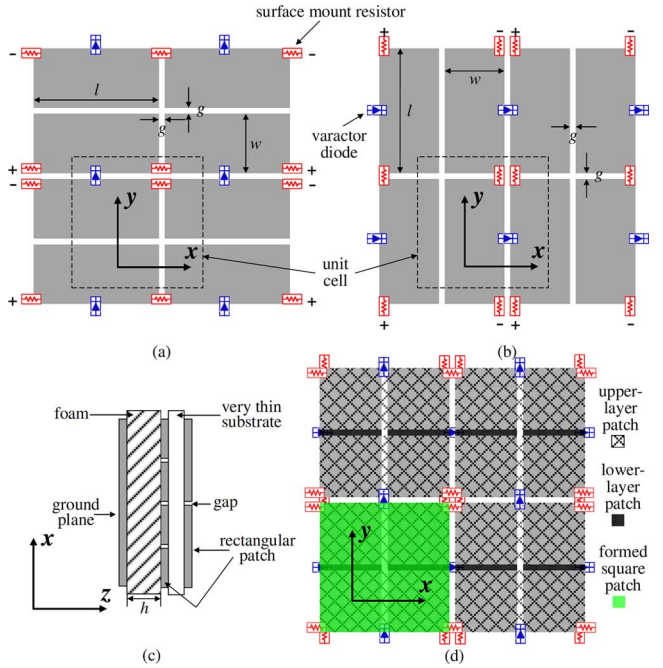

Fig. 1. Unit cells of the dual-polarized EBG structure with varactors and resistors. (a) Upper layer. (b) Lower layer. (c) Magnified cross-sectional view. (d) Alignment of the upper and lower layers.

Section II, the new EBG design and its wideband tuning characteristic are introduced. A wideband monopole antenna is placed above the EBG surface, achieving the conversion from LP to CP. By independently tuning the bias voltages on each side of the surface, the operating frequency to generate CP waves is tuned between 1–1.6 GHz. Also, the configuration provides the capability of agile polarization switching between LHCP and RHCP. The design can be used in applications of satellite navigation, covering the frequencies of GPS, GLONASS, COMPASS, Galileo, and IRNSS. The configuration and simulation results are presented in Section III, and measurement results are presented in Section IV, verifying the proposed functionalities. In Section V, the paper is concluded.

II. Dual-Polarized Tunable EBG Structure

In this section, the dual-polarized active EBG structure using rectangular patches is described. The patches are etched on both sides of a double metallic layer structure sandwiching a very thin polyester substrate Mylar. Fig. 1(a) and (b) illustrate the upper and lower layers of the EBG surface, and Fig. 1(c) shows the cross-sectional view of the whole structure, including the ground plane. A polystyrene foam ($\varepsilon_r = 1.04$) is sandwiched between the EBG surface and the ground plane, serving as a support of the flexible surface. The two patch layers of the EBG surface are identical but rotated by 90° from each other. The thickness of the Mylar is only 0.05 mm, so that the two periodic layers are isolated at direct current (DC). At radio frequencies (RF), the overlapping rectangular patches create square elements, as illustrated in Fig. 1(d). The dimensions are required to follow the relationship

$$l = 2w + g \tag{1}$$

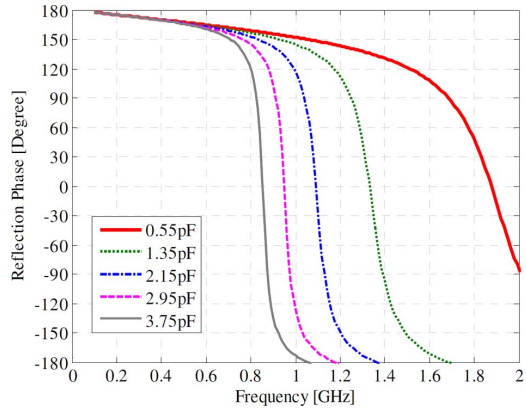

Fig. 2. Tuned reflection phase when C_2 is fixed to 0.55 pF and C_1 varies from 0.55 to 3.75 pF.

where l and w are the length and width of the rectangular patch respectively, and g is the width of the gap. As a result, the periodicity P is

$$p = l + g = 2w + 2g. \tag{2}$$

Specifically in this design, the dimensions in Fig. 1 are $w = 10$ mm, $g = 1$ mm, $l = 21$ mm, and $h = 5$ mm. On each layer, diodes are located between the longer sides of each pair of rectangles, while resistors are mounted in the corner between the shorter sides. This configuration allows for tuning rows and columns independently.

The diodes used were BB857 silicon varactors with a tunable capacitance range from 0.55 to 6.6 pF, according to the datasheet. The resistors were 10 kΩ.

The EBG structure was simulated by the frequency domain solver included in CST Microwave Studio, using the unit cell boundary condition. The mapping manner of the unit cell is shown in Fig. 1(a) and (b), with a periodicity $P = 22$ mm and a varactor and two resistors included in each layer. The diode was modeled as a RLC serial lumped element, with series resistance of 1.5 Ω and inductance of 0.6 nH, as well as the series variable capacitance. The reference plane was located 5 mm above the EBG surface. Here, the uniform capacitance of varactors in the upper layer is denoted by C_1, while the capacitance of the lower-layer varactors is C_2.

Fig. 2 presents the tuning capability of the EBG structure. When C_2 is fixed at 0.55 pF, and C_1 changes from 0.55 to 3.75 pF, a wide tuning range of the reflection phase is obtained for y-polarization. The reflection phase of the x-polarization remains stable at the value for $C_1 = 0.55$ pF. Alternatively, when C_1 is fixed and C_2 varied, the tuning characteristics are reciprocal. Therefore, the active EBG exhibits independent tuning ability for dual polarizations, and their respective reflection phases can be exchanged when swapping control of C_1 and C_2.

III. Wideband Monopole Antenna Above Dual-Polarized Tunable EBG Structure

A. Tuning Capability

The basic principle of converting LP to CP was presented in [9]. The omnidirectional LP antenna was positioned close to

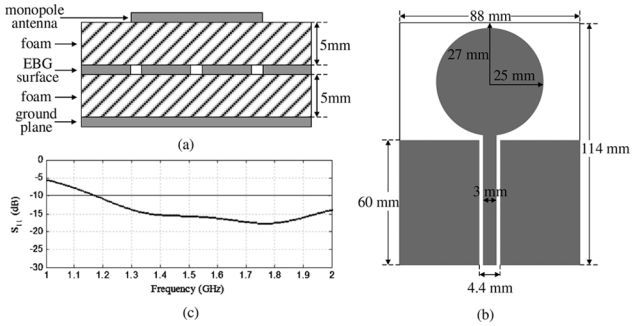

Fig. 3. Wideband monopole antenna above the dual-polarized tunable EBG structure. (a) Side view of the whole structure. (b) Top view of the monopole antenna. (c) Simulated S_{11} of the monopole.

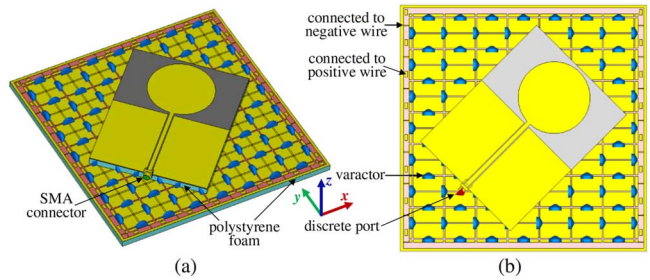

Fig. 4. Structure modeled in CST. (a) Perspective of the simulation model excluding resistors. (b) Top view of the simulation model excluding resistors.

the EBG surface, rotated by 45° with respect to the EBG lattice. The total radiation field ($\overrightarrow{E}$) along the $+z$-direction can be the composition of the field directly radiated from the antenna ($\overrightarrow{E}^d$) and the one reflected by the EBG structure ($\overrightarrow{E}^r$) as follows:

$$\begin{aligned}\overrightarrow{E} &= \overrightarrow{E}^d + \overrightarrow{E}^r \\ &= \frac{E_0}{2}(\hat{x}\cdot e^{-jkz} + \hat{y}\cdot e^{-jkz}) \\ &\quad + \frac{E_0}{2}(\hat{x}\cdot e^{-jkz-2jkd+j\theta_x} + \hat{y}\cdot e^{-jkz-2jkd+j\theta_y}) \end{aligned} \quad (3)$$

where E_0 is the magnitude of the electric fields, k is the wavenumber in free space, d is the height of the antenna over the EBG surface, θ_x and θ_y are the reflection phases of the EBG for the x- and y-polarized incident wave, respectively. When the antenna is placed very close to the EBG surface, the term $2\,kd$ is close to zero. Therefore, when $\theta_x = 90°$ and $\theta_y = -90°$, the total field becomes

$$\overrightarrow{E} = \frac{E_0}{2}\cdot e^{-jkz}[(\hat{x}+\hat{y}) + j(\hat{x}-\hat{y})] \quad (4)$$

so an RHCP wave is obtained. Similarly if $\theta_x = -90°$ and $\theta_y = 90°$, the wave will be LHCP. Note that in order to predict the antenna characteristics rigorously, the value of d should not be neglected, and complex factors must be considered, including the finitude of the EBG structure, as well as the interactions between the antenna and the EBG.

A coplanar waveguide (CPW) fed wideband monopole is used as the radiating antenna, so as to provide good input matching over the entire frequency band of satellite navigation. The monopole antenna uses a 0.787-mm-thick Rogers RT/Duroid 5870 dielectric substrate with a permittivity of 2.33 and a dielectric loss ($\tan\delta$) of 0.001. As shown in Fig. 3(a), it is located above the EBG surface in the center, with a distance h' of 5 mm. The dimensions of the monopole are presented in Fig. 3(b), and the simulated S_{11} is shown in Fig. 3(c).

The simulation model in CST is shown in Fig. 4. The EBG surface is composed of 7×7 unit cells and overall dimensions of 171 mm × 171 mm including the perimeter bias contacts. In each row/column of the EBG surface, the configuration of patches and resistors is designed to be symmetric, so that voltages can be added from both sides in practice. As a result, the voltage drop produced by the very small current flowing across the diodes was minor, as mentioned in [23], owing to the symmetry of the bias circuit. In simulations, the monopole antenna was fed by an SMA connector, excited by a discrete port. The time domain solver rather than the frequency domain solver included in CST was used for the simulations, to avoid the unacceptably large memory and computing time required by the latter solver.

In the tuning process, the lower limit of C_1 (or C_2) is 0.55 pF according to the tunable capacitance range of the BB857 varactor diode. Through tuning the other capacitance C_2 (or C_1) to another specific value, the highest operation frequency of the antenna to realize CP waves is determined. This frequency is also adjustable by changing the dimensions of the structure, such as varying the height of the foam between the EBG surface and the ground plane, which will be discussed in Section V. In the present design, the entire structure including the monopole was optimized to achieve the highest working frequency of 1.60 GHz. By means of tuning C_1 and C_2 together, the working frequency can be tuned to any value within the desired range.

Fig. 5(a) presents the simulated results of AR at $\theta = 0°$, $\varphi = 0°$ and Fig. 5(b) presents S_{11} versus frequency, demonstrating the tuning capability of the antenna. It can be seen that good ARs were realized at six arbitrarily selected frequencies between 1.10 and 1.60 GHz, with 3 dB AR bandwidths of 1.3%, 1.9%, 2.2%, 2.9%, 3.5%, and 3.5%, respectively. Each AR curve was obtained by adjusting C_1 and C_2 to a specific pair of values, which provides flexibility and precision of tuning to achieve satisfactory CP characteristics at any desired frequency within the dynamic range. Therefore, the simulated AR bandwidth is 40% (1.09–1.63 GHz) in total. The corresponding simulated S_{11} of each case are shown in Fig. 5(b) and as observed for the AR curves, the operating frequencies of S_{11} decrease as the capacitances grow, and the value is less than -10 dB at each working frequency in Fig. 5(a). The radiation patterns at 1.6 and 1.1 GHz are shown in Fig. 6 and were not found to vary greatly with frequency. In both the x–z and the y–z planes, LHCP radiation patterns were realized, with low cross polarizations, i.e., RHCP.

B. *Effect of Tuning C_1 and C_2*

The ability to tune working frequencies continuously over the operating band is indispensable for the concept of broadband realization. By tuning C_1 and C_2 together, good AR can be obtained at any specific frequency. Although adjusting two

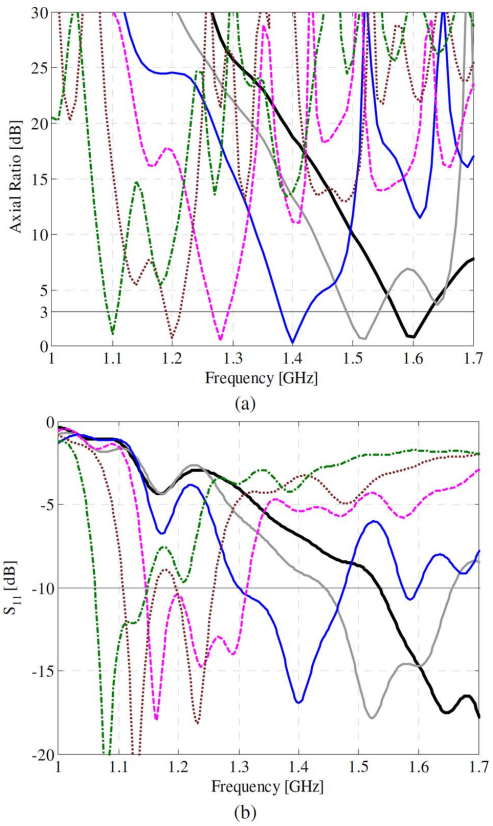

Fig. 5. Simulation results to show the tuning capability. (a) Axial Ratio (AR). (b) S_{11}.

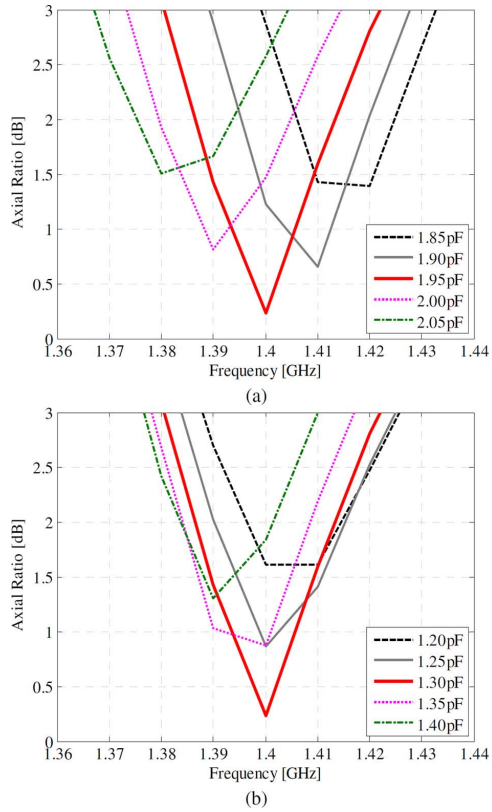

Fig. 7. Effect of varied capacitances on AR. (a) C_1 fixed to 1.30 pF, C_2 varied. (b) C_2 fixed to 1.95 pF, C_1 varied.

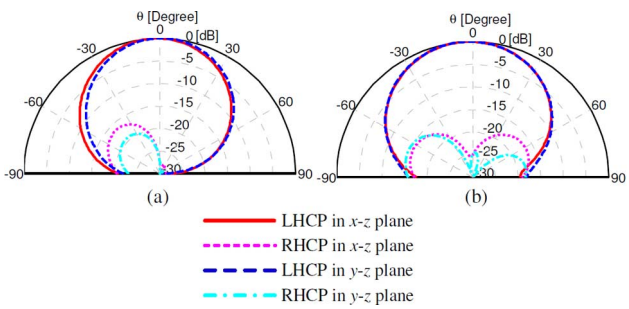

Fig. 6. Simulated radiation patterns. (a) 1.60 GHz. (b) 1.10 GHz.

parameters together seems to be much more complicated than one-dimensional tuning, varying C_1 and C_2 individually makes it straightforward to achieve high quality AR at any desired frequency. As shown in Fig. 7(a), when C_1 is fixed to 1.30 pF, and C_2 is varied between 1.85 and 2.05 pF, the AR curves shift to lower frequency domain. Along with the increase of C_2, the best AR of each curve declines gradually, and sinks to the lowest point before continuing to rise up. This suggests that the AR curve can be tuned to a fairly low level at a certain frequency, by gradually increasing or reducing C_2. Fig. 7(b) presents the effect of varying C_1 from 1.20 to 1.40 pF, while fixing C_2 to 1.95 pF. It is observed that the effects are almost the same as those shown in Fig. 7(a), except for smaller frequency shifts caused by the same increment of capacitance. As indicated in Fig. 2, the curve of the reflection phase shifts towards lower frequencies and becomes steeper as the capacitance increases, resulting in the reflection phase more sensitive to the variation of capacitance in lower frequencies. Therefore, the same increment of C_2 causes a notably larger difference of reflection phase than C_1, consequently the AR becomes more sensitive to the change of C_2 than C_1, as illustrated in Fig. 7. In general, tuning an AR curve to a low level at a desired frequency can be realized by alternatively varying C_1 and C_2, on the basis of the tuning effects shown and described. It has been found that such a tuning guide is not only effective in simulations, but in measurement as well. Fig. 8 suggests that although the lowest value of S_{11} may not coincide exactly with the best AR frequency, the S_{11} bandwidth is sufficiently large that the antenna remains well matched over the whole 3 dB AR bandwidth. In other words, as long as the AR is tuned to a satisfactory level at the desired frequency, good antenna matching can be obtained inherently, which is also verified by Fig. 5. Therefore, AR rather than S_{11} is the crucial characteristic to be concerned within the tuning process.

C. Switching Between LHCP and RHCP

Besides the frequency reconfigurability, the ability of switching between LHCP and RHCP is the other feature of this design. Simulated results of the case working at 1.40 GHz are used as a demonstration. Owing to the symmetry of the structure, the AR curves of the two cases with swapped C_1 and C_2 overlap perfectly, as do the S_{11} curves, as shown in Fig. 9. Also, the radiation patterns in Fig. 10(b) are almost identical to those in Fig. 10(a), but RHCP has been obtained, as opposed to LHCP. Therefore, the reconfigurability of polarizations can be conveniently realized, by swapping the varactor capacitances

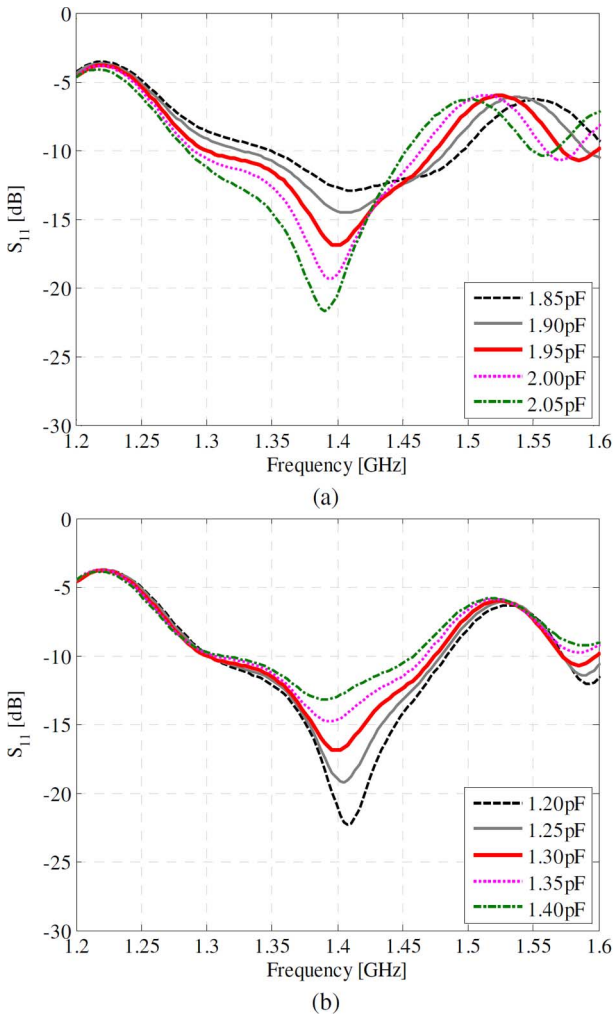

Fig. 8. Effect of varied capacitances on S_{11}. (a) C_1 fixed to 1.30 pF, C_2 varied. (b) C_2 fixed to 1.95 pF, C_1 varied.

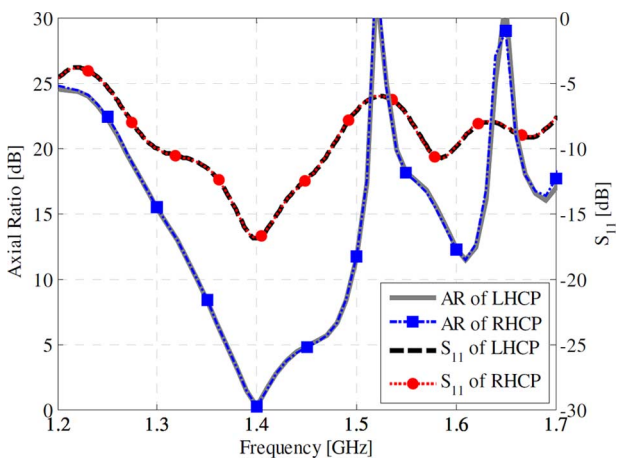

Fig. 9. Effect of swapping $C_1 = 1.30$ pF and $C_2 = 1.95$ pF on AR and S_{11}.

on the two layers, i.e., the supplied DC voltages in practical measurement.

IV. Fabrication and Measurement

Photographs of the fabricated prototype are shown in Fig. 11. Surface mount BB857 varactors and resistors of 10 kΩ were sol-

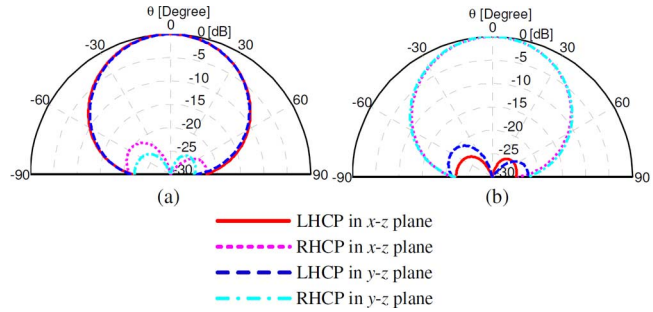

Fig. 10. Effect of swapping $C_1 = 1.30$ pF and $C_2 = 1.95$ pF on radiation patterns.

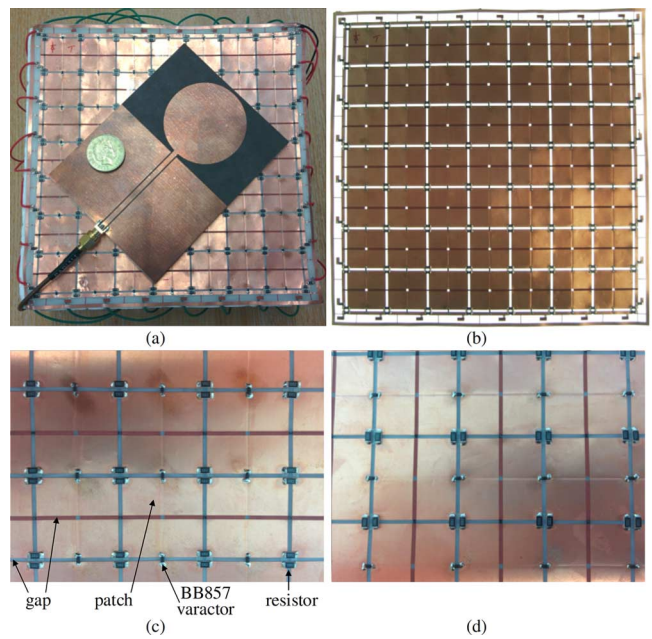

Fig. 11. Photographs of the prototype. (a) Entire structure. (b) Top view of the entire EBG surface. (c) Enlarged top layer of the EBG surface. (d) Enlarged bottom layer of the EBG surface.

dered on both sides of the EBG surface. On the upper layer, red wires were connected to both sides of terminals to provide positive DC power denoted by U_1, while on the lower layer green wires were employed and the voltage was U_2. To simplify the structure and reduce the number of DC wires, the negative terminals of each layer were connected to conducting strips on the boundary. In the measurement, the two voltages were independently tunable, by using two power supplies with the range of 0–30 V at a precision of 0.01 V. As predicted, the measured voltage drop was about 0.1%, which exerts minor impact on the antenna performance.

Based on the tuning guide in Section III-B, the ARs at $\theta = 0°$, $\varphi = 0°$ were measured in an anechoic chamber, and the curves were tuned to good AR values at six randomly chosen frequencies between 1.04 and 1.52 GHz, respectively, as presented in Fig. 12(a). The 3dB AR bandwidth of each curve is 1.6%, 1.4%, 1.9%, 2.6%, 3.4%, and 2.8%, respectively. Owing to the capability of precise tuning over the entire frequency band, the 3 dB AR bandwidth reached about 40% (1.03–1.54 GHz) in total. The six curves correspond to the cases from A to F listed in Table I,

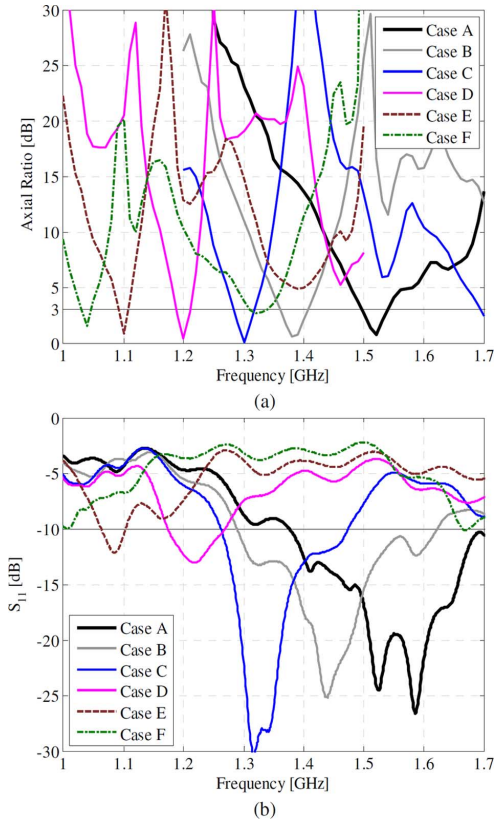

Fig. 12. Measured AR and S_{11} of the antenna. (a) Tunable AR characteristics. (b) S_{11} in the corresponding cases of (a).

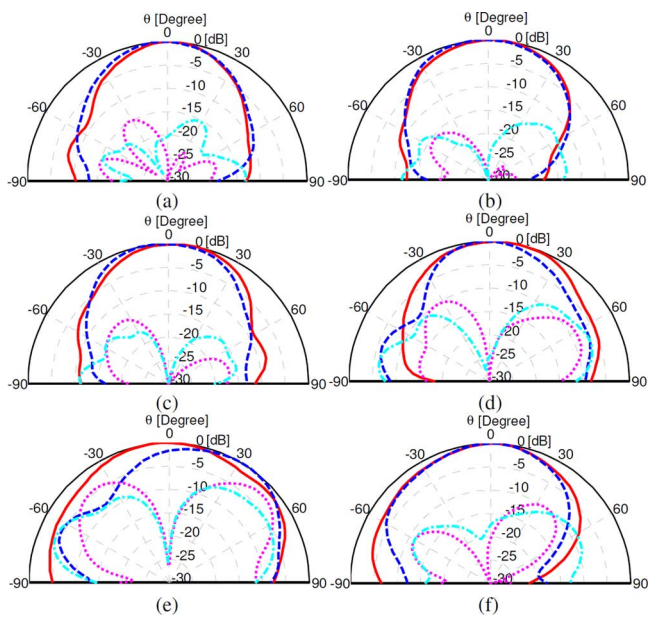

Fig. 13. Measured radiation patterns of different cases. (a) Case A @1.52 GHz. (b) Case B @1.38 GHz. (c) Case C @1.30 GHz. (d) Case D @1.20 GHz. (e) Case E @1.10 GHz. (f) Case F @1.04 GHz.

and voltage supplies of each case in measurement are also provided. S_{11} of these cases are shown in Fig. 12(b), which were all less than -10 dB at the working frequencies except Case F. At 1.04 GHz, S_{11} was -8.2 dB, as the monopole antenna was not as well matched as at higher frequencies. In Case G, S_{11} was greatly deteriorated by the EBG structure, when the power

TABLE I
TUNING CHARACTERISTICS OF DIFFERENT CASES

	U_1 (Volt)	U_2 (Volt)	Frequency (GHz)	Polarization
Case A	29.50	10.68	1.52	LHCP
Case B	13.23	7.39	1.38	LHCP
Case B*	7.39	13.23	1.38	RHCP
Case C	9.62	6.18	1.30	LHCP
Case C*	6.18	9.62	1.30	RHCP
Case D	6.95	4.91	1.20	LHCP
Case E	5.73	3.53	1.10	LHCP
Case F	4.98	2.36	1.04	LHCP
Case G	0	0		LP

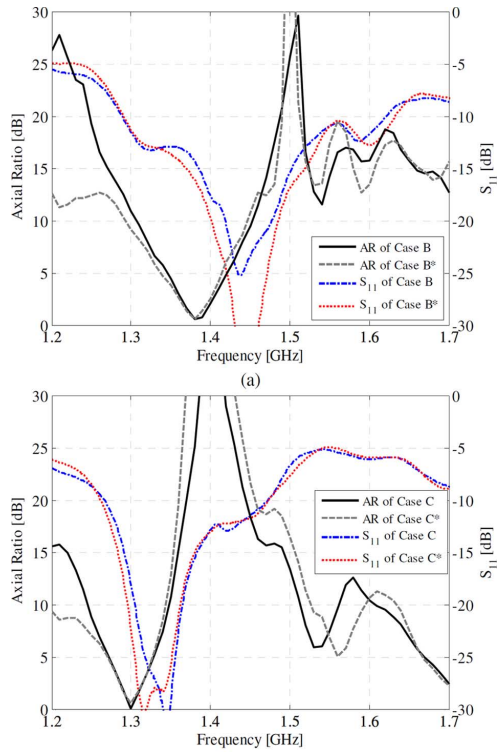

Fig. 14. Comparison of the measured AR and S_{11} between switched cases. (a) Cases B and B*. (b) Cases C and C*.

supplies were off. The radiation patterns at the six frequencies listed in Table I were measured in the x–z and the y–z planes, and are shown in Fig. 13. Although the patterns show generally good LHCP characteristics, the cross-polarization (RHCP) near the zenith angle in some cases are not as low as obtained in simulations. This may be due to the fabrication and measurement errors, as well as the effect of the feeding cable.

To verify the polarization reconfigurability of the structure, Case B* and C* were implemented in the measurement, by repeating Case B and C in turn but swapping U_1 and U_2 in each case. The AR and S_{11} curves versus frequency are shown in Fig. 14. Although small differences are observed due to the asymmetry and misalignment in fabrication and measurement, good agreement of curves between the original cases and the star cases is obtained, especially near the CP operating frequencies. The radiation patterns at 1.38 GHz of Case B* and at 1.30 GHz of Case C* are shown in Fig. 15(a) and(b), respectively. In contrast with Fig. 13(b) and (c), *RHCP* patterns as the co-polarization are obtained, by simply swapping U_1 and U_2.

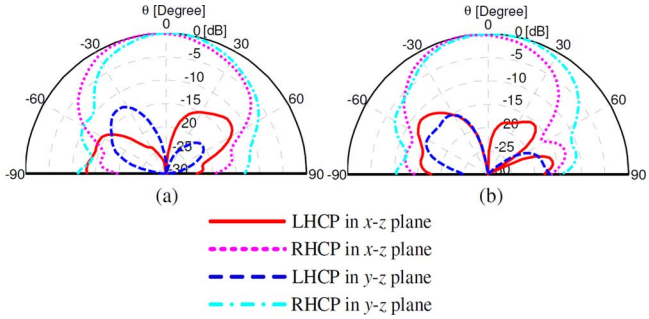

Fig. 15. Radiation pattern of the switched cases. (a) Case B* @1.38 GHz. (b) Case C* @1.30 GHz.

V. Discussion

Frequency and polarization reconfigurability of a tunable EBG reflector based antenna has been realized by both simulations and measurements. The highest operating frequency was 1.52 GHz in the measurement with a drift of 5% compared to 1.60 GHz in simulation. The difference could be caused by general fabrication (e.g., etching, masks alignment, soldering of components) and measurement errors, as well as the following factors.

First, the varactor capacitances grow gradually as the frequency increases, as discussed in [15]. When biased by the same voltage, the practical capacitances were higher at the frequencies of interest than those provided in the datasheet at 1 MHz, resulting in lower working frequencies than expected in the simulation. Similar frequency shifts were also found in [23], incorporating the same BB857 varactor diodes.

Second, the fabrication accuracy of cutting polystyrene foam was not as good as the etching technique, making the used foams 0.4 mm thicker than the design. As shown in Fig. 3, foams were employed to space the EBG surface from the lower ground plane and the upper monopole antenna respectively. Simulation studies suggested that the matching and radiating performances were insensitive to the value of h', with the variation range from 4 to 6 mm, while the effect of h was found to be significant. Fig. 16 presents the parametric study of h in terms of the AR and S_{11}. As the value increases from 4.0 to 6.0 mm, the AR frequency drops from 1.69 to 1.52 GHz, and the S_{11} curve shifts towards the low frequency domain as well. Therefore, the 0.4 mm increase of the foam thickness is believed to contribute to the frequency reduction considerably.

Third, the full physical geometrical shapes of the varactors and resistors, and also the wires at the end of the bias lines, were not accounted for in the simulations. Note that additional resistors were added at the edges to further isolate RF signals (see Fig. 11(a)), and minimize the effect of the perimeter bias lines.

VI. Conclusion

A novel dual-polarized tunable EBG structure has been presented, which is incorporated in the design of a frequency and polarization reconfigurable CP antenna. The EBG surface employs a very thin polyester substrate with periodic metallic rectangular patches cladding on its two sides. Varactors are placed in the vertical and the horizontal directions on each side respectively, enabling the reflection phase of the dual polarizations to be tuned independently. Resistors of 10 kΩ are used to directly connect adjacent patches, simplifying the bias circuits and minimizing the voltage drops. A CPW fed monopole antenna is placed above the EBG structure, generating CP waves based on the principle of using PDEBG to convert the linear polarization into the circular polarization. Owing to the independently tunable capability of the EBG, CP waves could be realized at any desired frequency over a broad band, by together adjusting the two sets of bias voltages which respectively control the varactor capacitances on each layer. The configuration also enables the radiation patterns to be switched agilely between LHCP and RHCP, realizing the polarization reconfigurability. To clarify the tuning principle and provide a guide for the tuning process, the effects of the loaded capacitances are discussed. The antenna exhibits a 3 dB AR bandwidth of 40% in simulation and practice, which is significantly increased compared with the value of 25.2% achieved by the broadband antenna using passive EBG structure in [11]. In our case, the antenna height is only $0.046\lambda_0$ (10.787 mm, $f_0 = 1.285$ GHz), showing a considerable reduction of profile compared with the previously reported value of $0.101\lambda_0$ (4.8 mm, $f_0 = 6.315$ GHz) [11]. In addition, the switching function between LHCP and RHCP is realized as well. Owing to the broadband characteristic of the monopole antenna and the tunable ability of the EBG structure, good matching is achieved at each tuned case. This antenna can be used in the applications of many operational and in-development global navigation systems, including GPS, GLONASS, COMPASS, Galileo, and IRNSS.

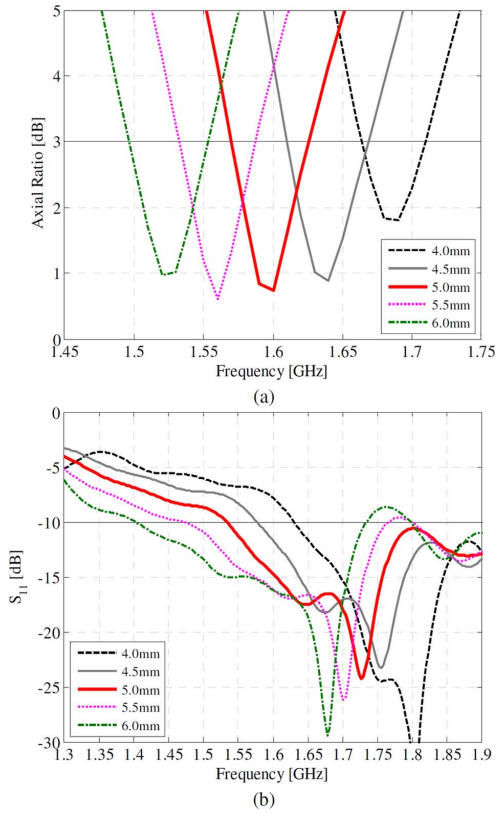

Fig. 16. Effect of the distance between the EBG surface and the ground plane on (a) AR and (b) S_{11}.

REFERENCES

[1] Y. Rahmat-Samii, "Electromagnetic band-gap structures: Classification, characterization, and applications," in *Proc. 11th Int. Conf. Antennas Propag.*, 2001, pp. 560–564, (IEE Conf. Publ. No. 480).

[2] A. S. Barlevy and Y. Rahmat-Samii, "Characterization of electromagnetic band-gaps composed of multiple periodic tripods with interconnecting vias: Concept, analysis, and design," *IEEE Trans. Antennas Propag.*, vol. 49, no. 3, pp. 343–353, Mar. 2001.

[3] D. Sievenpiper, L. Zhang, R. F. Broas, N. G. Alexopolous, and E. Yablonovitch, "High-impedance electromagnetic surfaces with a forbidden frequency band," *IEEE Trans. Microw. Theory Techn.*, vol. 47, no. 11, pp. 2059–2074, Nov. 1999.

[4] F. Yang and Y. Rahmat-Samii, "Reflection phase characterizations of the EBG ground plane for low profile wire antenna applications," *IEEE Trans. Antennas Propag.*, vol. 51, no. 10, pt. 1, pp. 2691–2703, Oct. 2003.

[5] F. Yang and Y. Rahmat-Samii, "Microstrip antennas integrated with electromagnetic band-gap (EBG) structures: A low mutual coupling design for array applications," *IEEE Trans. Antennas Propag.*, vol. 51, no. 10, pt. 2, pp. 2936–2946, Oct. 2003.

[6] J. M. Bell and M. F. Iskander, "A low-profile Archimedean spiral antenna using an EBG ground plane," *IEEE Antennas Wireless Propag. Lett.*, vol. 3, pp. 223–226, 2004.

[7] H. Nakano, K. Kikkawa, N. Kondo, Y. Iitsuka, and J. Yamauchi, "Low-profile equiangular spiral antenna backed by an EBG reflector," *IEEE Trans. Antennas Propag.*, vol. 57, no. 5, pp. 1309–1318, May 2009.

[8] F. Yang and Y. Rahmat-Samii, "Polarization dependent electromagnetic band gap (PDEBG) structures: Designs and applications," *Microw. Opt. Technol. Lett.*, vol. 41, pp. 439–444, 2004.

[9] F. Yang and Y. Rahmat-Samii, "A low profile single dipole antenna radiating circularly polarized waves," *IEEE Trans. Antennas Propag.*, vol. 53, no. 9, pp. 3083–3086, Sep. 2005.

[10] H. Yi and S.-W. Qu, "A novel dual-band circularly polarized antenna based on electromagnetic band-gap structure," *IEEE Antennas Wireless Propag. Lett.*, vol. 12, pp. 1149–1152, 2013.

[11] T. Nakamura and T. Fukusako, "Broadband design of circularly polarized microstrip patch antenna using artificial ground structure with rectangular unit cells," *IEEE Trans. Antennas Propag.*, vol. 59, no. 6, pt. 2, pp. 2103–2110, Jun. 2011.

[12] L. Boccia, F. Venneri, G. Amendola, and G. Di Massa, "Application of varactor diodes for reflectarray phase control," in *Proc. Antennas Propag. Soc. Int. Symp.*, 2002, p. 132.

[13] D. Sievenpiper and J. Schaffner, "Beam steering microwave reflector based on electrically tunable impedance surface," *Electron. Lett.*, vol. 38, pp. 1237–1238, 2002.

[14] D. F. Sievenpiper, J. H. Schaffner, H. J. Song, R. Y. Loo, and G. Tangonan, "Two-dimensional beam steering using an electrically tunable impedance surface," *IEEE Trans. Antennas Propag.*, vol. 51, no. 10, pt. 1, pp. 2713–2722, Oct. 2003.

[15] C. Mias and J. H. Yap, "A varactor-tunable high impedance surface with a resistive-lumped-element biasing grid," *IEEE Trans. Antennas Propag.*, vol. 55, no. 7, pp. 1955–1962, Jul. 2007.

[16] C. Mias, "Varactor-tunable frequency selective surface with resistive-lumped-element biasing grids," *IEEE Microw. Wireless Compon. Lett.*, vol. 15, pp. 570–572, 2005.

[17] H. J. Lee, R. Langley, and K. Ford, "Tunable active EBG," in *Proc. 2nd Eur. Conf. on Antennas Propag.*, Nov. 11–16, 2007, pp. 1–4.

[18] H. J. Lee, K. Ford, and R. Langley, "Dual band tunable EBG," *Electron. Lett.*, vol. 44, pp. 392–394, 2008.

[19] H. J. Lee, "Independent multiband antenna tuning using an active EBG," in *Proc. Loughborough Antennas Propag. Conf.*, 2008, pp. 141–144.

[20] B. Sanz-Izquierdo, E. A. Parker, J. B. Robertson, and J. C. Batchelor, "Tuning technique for active FSS arrays," *Electron. Lett.*, vol. 45, pp. 1107–1109, 2009.

[21] B. Sanz-Izquierdo, E. A. Parker, J. B. Robertson, and J. C. Batchelor, "Tuning patch-form FSS," *Electron. Lett.*, vol. 46, pp. 329–330, 2010.

[22] B. Sanz-Izquierdo, E. A. Parker, and J. C. Batchelor, "Dual-band tunable screen using complementary split ring resonators," *IEEE Trans. Antennas Propag.*, vol. 58, no. 11, pp. 3761–3765, Nov. 2010.

[23] B. Sanz-Izquierdo and E. A. Parker, "Dual polarized reconfigurable frequency selective surfaces," *IEEE Trans. Antennas Propag.*, vol. 62, no. 2, pp. 764–771, Feb. 2014.

Bin Liang received the B.Sc. degrees in electronic and information engineering from Beihang University (Beijing University of Aeronautics and Astronautics, BUAA), Beijing, China, in 2008. He is currently pursuing the joint Ph.D. degree from Beihang University, China, and the University of Kent, Kent, U.K.

Since 2012, he has been a Ph.D. student visitor at the University of Kent, funded by the China Scholarship Council (CSC). His research interests include frequency selective surfaces, electromagnetic band-gap structures, and computational electromagnetic.

Benito Sanz Izquierdo received the B.Sc. degree from the University of Las Palmas de Gran Canaria, Las Palmas, Spain, and the M.Sc. and Ph.D. degrees from the University of Kent, Kent, U.K., in 2002 and 2007, respectively.

From 2003 to 2012, he was a Research Associate with the School of Engineering and Digital Arts, University of Kent, and in 2013, became a lecture in electronic systems. In 2012, he spent some time working for Harada Industries Ltd., where he developed novel antennas for the automotive industry. His research interests include multiband antennas, wearable microwave devices, substrate integrated waveguides components, electromagnetic band-gap structures, and frequency selective surfaces.

Edward (Ted) Parker received the M.A. degree in physics and Ph.D. degree in radio astronomy from Cambridge University (St. Catharine's College), Cambridge, U.K.

He was appointed Reader at the University of Kent in 1977, and since 1987 he has been Professor of Radio Communications, now Professor Emeritus. He established the Antennas Group in the Electronics Laboratory, University of Kent, Kent, U.K. The early work of that group focused on reflector antenna design, later on frequency selective surfaces and patch antennas. One of his interests is the study and overhaul of antique clocks.

Dr. Parker is a member of the IET.

John C. Batchelor (S'93–M'95–SM'07) received the B.Sc. and Ph.D. degrees from the University of Kent, Canterbury, U.K., in 1991 and 1995, respectively.

From 1994 to 1996, he was a Research Assistant with the Electronics Department, University of Kent, and in 1997, became a Lecturer of electronic engineering. He now leads the Antennas Group at Kent and is a Reader in Antenna Technology. His current research interests include UHF RFID tag design, passive sensing, body-centric antennas, printed antennas, compact multiband antennas, electromagnetic bandgap structures, and long-wavelength FSS (frequency-selective surfaces).